J. Fluid Mech. (1989), *vol.* 199, *pp.* 29–53
Printed in Great Britain

The growth of compositionally stratified solid above a horizontal boundary

By ANDREW W. WOODS AND HERBERT E. HUPPERT
Department of Applied Mathematics and Theoretical Physics, University of Cambridge, Silver Street, Cambridge, CB3 9EW, UK

(Received 12 June 1987 and in revised form 1 June 1988)

The compositional stratification in solid formed by cooling a binary alloy from below is investigated theoretically and experimentally. It is shown that in order to grow composite solid the boundary temperature needs to be below the eutetic temperature. Two separate cases are considered. In the first, heavy fluid is released on solidification. The solid growth is then governed by the diffusive transport of heat and composition. The resultant solid is shown to have a fixed composition until the far-field conditions change. In the second case, light fluid is released on solidification. This generates turbulent compositional convection in the melt which significantly increases the transport of heat and composition across the solid/melt interface. As a result, the fraction of heavy component in the solid initially increases, but subsequently decreases to conserve mass. A simple theoretical model, using the approximation of a flat solid/melt interface is developed; this predicts differences in the thermal flux in saturated and undersaturated melts. Laboratory experiments involving aqueous solutions of sodium carbonate cooled from below which released light fluid displayed compositional convection and stratification of the solid as predicted.

1. Introduction

The mechanisms by which compositional variations are generated by the solidification of multi-component melts are important in many fields. These include geology, metallurgy and materials science. In the geological context, interest centres on solidified magma chambers, which often exhibit significant spatial variation in the composition of the solid. These magma chambers originally contained molten magma, which may have entered the chamber as a well-mixed fluid and solidified progressively.

In this work, we address the thermodynamic and fluid-dynamic processes which lead to the formation of a compositionally stratified solid. In order to bring out the essential details, we consider simple solidification situations in which solid is grown on a planar surface from a binary (two component) melt. We have conducted a number of laboratory experiments in which well-mixed aqueous salt solutions were solidified by cooling at a planar surface. Depending upon the position of the cooling plate and the melt composition a number of different solid compositional profiles were obtained. The fluxes of solute and temperature are critical to the determination of the solid composition. As the inclination to the horizontal of the planar surface on which the solid grows is varied, a wide range of fluid motions, driven by buoyancy, occurs in the melt. These cause significant differences in the transport of heat and composition and thus the resulting stratification of the solid (Leitch 1985; Huppert *et al.* 1987).

The majority of previous studies in the field, summarized in the monographs by Elliott (1983) and Kurz & Fisher (1986), have adopted one of two approaches. The first assumes that all transport in the melt is governed by diffusion and effectively ignores the crucially important role of fluid flow. The second assumes that the solute rejected on solidification is instantly mixed into the remaining melt by highly efficient fluid motions, resulting in the lever-rule or Scheil equation governing the solid composition. Further, in many of these studies the solid grown is assumed to be of one phase only; its composition varies only because the solidus line is in general non-vertical (see §2). However, in the present study, we consider the compositional stratification formed in composite solid in which crystals of both phases are mutually intertwined.

The first part of this study, which forms the basis of the present paper, considers the solidification of a binary melt above a horizontal, cooled boundary. First, we describe a general thermodynamic equilibrium model for the solidification of a binary melt, based on a eutectic phase diagram. In §3 we consider briefly solidification of a melt accompanied by the release of heavy fluid. This is a process controlled by diffusion and our approach extends the model of Huppert & Worster (1985) and Worster (1986). In §4 we describe the solidification of a melt which releases light fluid. We derive a model for the compositional and thermal fluxes at the solid/melt interface which are produced by compositional convection. We then compare predictions of the model with laboratory experiments we have conducted. In §6, we present a brief discussion of the possible application of the results to magma chambers. In the concluding section we summarize the various types of solid stratification that can be produced by solidification above a horizontal boundary maintained at a fixed temperature.

2. Solidification above a cooled horizontal boundary

2.1. *Phase diagram*

We assume that the solidification of a binary melt is governed by equilibrium thermodynamics; this means that the solidification is thermodynamically quasi-static and that the time taken for the system to evolve is much greater than the time taken to readjust to thermodynamic equilibrium at any stage. Under these conditions, the thermodynamics is described by a phase diagram, such as the one shown in figure 1. Above AEB the system is totally liquid; a state which we refer to as the melt. In the two triangular regions AEA′ and BEB′ the melt coexists with either pure solid A or B. The point E is the eutectic point; below the horizontal line through this point (the eutectic line) no melt can exist. At the eutectic temperature, melt in thermodynamic equilibrium can only have the eutectic composition.

From this diagram we can immediately deduce two results. First, that (non-dendritic) composite eutectic solid may only be grown when the solid/melt interface temperature, T_i, is the eutectic, T_e (ignoring the very small local temperature variations due to the variable crystal curvature (Elliott 1983)). In fact this temperature will be just below eutectic, in order that a phase change will occur, but we assume that this effect is negligible (Langer 1980; Kurz & Fisher 1986). By the same argument, when growing solid behind a mush phase, the temperature at the solid/mush interface is at the eutectic temperature.

Second, in order to drive the heat transfer in the system, the cooling boundary must be below the eutectic temperature, because the temperature at the solid/melt or solid/mush boundary is eutectic. This undercooling produces a heat transfer

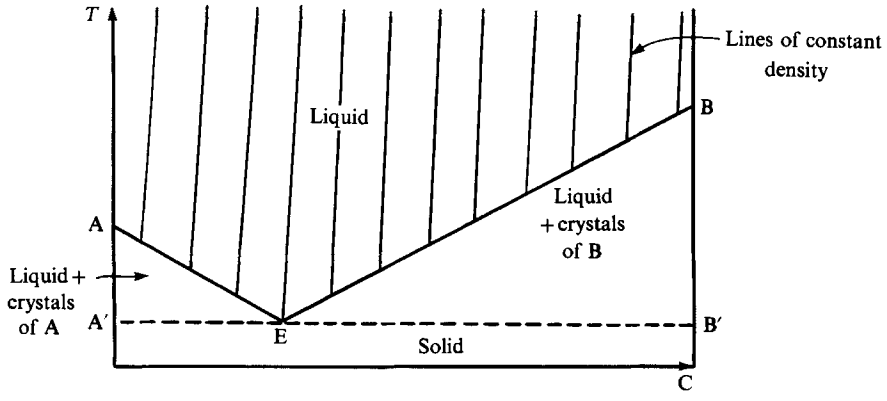

FIGURE 1. Phase diagram of a binary alloy. AE and EB are the liquidus lines, A′EB′ is the eutectic line. The line AA′ corresponds to pure solid A and the line BB′ to pure solid B.

across the solid which is balanced by the production of enthalpy of fusion and the heat flux from the melt generated by its cooling.

2.2. *Density*

The density of the melt increases with the mass fraction of component B, and decreases with temperature. As is usually the case, the lines of constant density are almost vertical (figure 1) reflecting the fact that the influence of composition on density is generally much stronger than that of temperature. This density relationship causes different types of buoyancy driven motions in the melt during the solidification process. These motions alter the heat and solute fluxes at the solid/melt interface. To avoid confusion, in the remainder of the paper we only refer to mass fluxes of component B, and describe them as compositional fluxes.

2.3. *Solid morphology*

When composite solid forms, the solid/melt interface may be approximately flat, with small deviations arising owing to the curvature of the crystals. Alternatively, the interface may be unstable and dendrites may form (Elliott 1983). We refer to the former as a 'flat' interface; this contrasts with the truly flat (i.e. planar) interface which can form when only one phase solidifies. We now consider briefly the morphology of the composite solid that forms with each of these types of interface.

If the solid/melt interface is approximately flat and horizontal the solidification problem is effectively one-dimensional. In such morphologically stable growth, the melt composition and temperature at the interface together with the heat and mass fluxes across the interface determine whether either single-phase solid of pure component A or pure component B or composite eutectic solid forms. In composite eutectic solid the crystals of each phase either grow in adjacent planes forming a lamellar structure, or when there is a greater quantity of one component than the other in the solid, rod-like crystals of the minor component grow in a matrix of the major component. There is a range of compositions, around the eutectic composition, in which composite eutectic solid is morphologically stable (for example Mollard & Flemings 1967 grow Pb–Sn solid with the Pb content ranging from 12% to 26%); however, when the solid composition becomes too far removed from the eutectic composition, composite eutectic solid growth is not possible.

If the solid growth is morphologically unstable, a mush phase will develop between

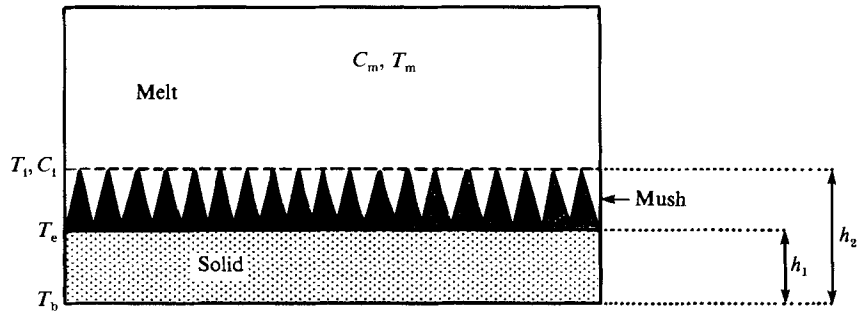

FIGURE 2. Schematic of a mushy interface.

the solid and the melt. The mush phase consists of dendritic, needle-shaped crystals extending from the solid, between which there is interstitial melt (figure 2). The dendritic crystals are all either of composition A or B depending whether the melt composition is above or below eutectic. We assume that the interstitial melt is in equilibrium and lies on the liquidus (lines AE and BE of figure 1). The solid front advances into the mush, by solidifying the interstitial melt, producing a matrix of composite eutectic solid around the dendritic crystals.

2.4. *Morphological stability*

At a certain degree of constitutional supercooling, dendritic growth involves a smaller degree of undercooling than flat interface growth, and so the planar interface breaks down. This principle was first expressed in a quantitative form by Mullins & Sekerka (1964). They derived

$$k_s \frac{\partial T}{\partial z}\bigg|_- + k_m \frac{\partial T}{\partial z}\bigg|_+ < m(k_m + k_s)\frac{\partial C}{\partial z}\bigg|_+ \tag{2.1}$$

as the criterion for instability of the one-dimensional steady-state, diffusively governed growth of a single phase solid, where k_s is the thermal conductivity in the solid, k_m that in the melt, T is the temperature, m the liquidus slope, C the mass fraction of component B present and z increases away from the interface, in the melt. Further stability studies have been carried out for more complex growth situations (see Elliott 1983; Kurz & Fisher 1986). The criterion for stability

$$\psi \frac{m_\alpha m_\beta}{(m_\alpha + m_\beta)} \frac{\partial C}{\partial z}\bigg|_+ < \frac{k_s \dfrac{\partial T}{\partial z}\bigg|_- + k_m \dfrac{\partial T}{\partial z}\bigg|_+}{k_s + k_m}, \tag{2.2}$$

where ψ is a complicated expression involving the liquidus slopes and the supercooling such that $\psi \approx 2$ and m_α and m_β are the two liquidus slopes at the eutectic point, was derived by Hurle & Jakeman (1968) for the steady-state, diffusively governed growth of a composite eutectic solid. This applies to the case in which one of the phases facets and has a form similar to that of the Mullins & Sekerka criterion (2.1).

Determination of the conditions for the onset of morphological stability in a convecting melt is difficult, especially in chaotic vigorous convection. The coupling of morphological and convective instability is analysed by Corriell *et al.* (1981) and Hurle, Jakeman & Wheeler (1982). However these analyses are completely linear and do not cover the case of turbulent convection at high Rayleigh number in the melt.

2.5. *Solid composition*

The composition of composite solid is given by the horizontal average of the quantity of solid phases A and B deposited. For a solid grown behind a mush zone, we define the composition at any depth in the solid in terms of the horizontally averaged composition, averaged over a scale larger than the dendritic crystal size. The dendritic crystals in the mush consist of either pure solid A or B, depending on whether the composition of the melt is less than or greater than eutectic, while the composition of the composite eutectic solid matrix can vary with space and time. Therefore the bulk solid composition may vary with depth in the solid if either the solid fraction in the mush at the solid/mush interface varies with time and/or the composition of the composite eutectic solid varies with time and therefore depth.

2.6. *Sub- and supereutectic melts*

There are three cases of interest when solid is grown above a horizontal boundary (Huppert & Worster 1985). Case I corresponds to cooling a melt of composition less than eutectic – a subeutectic melt. The melt at the solid/melt or solid/mush interface is heavy and cold and so is gravitationally stable. No fluid motions develop and the growth is controlled by diffusion (Huppert & Worster 1985; Worster 1986). Case II corresponds to cooling a melt of composition greater than eutectic – a supereutectic melt. The melt at the solid interface is now depleted in component B, and so may be light even though cold. For sufficiently large Rayleigh numbers, convection will then occur in the melt. The motion can significantly alter the fluxes of component B and of heat from those of the purely diffusive case. Case III corresponds to cooling a melt of eutectic composition. The solid grown also has eutectic composition. Therefore, stratified solid cannot form from such a melt, and we do not consider it further. Sidewall effects have not been included in the present work because they are only important if the container is relatively deep compared to its width, especially when the melt is well mixed by vigorous solutal convection (Adornato & Brown 1987).

For case I we consider diffusion-governed models for the growth of composite solid in both the morphologically stable, flat-interface case and in the morphologically unstable case when solidification occurs through a mush phase. For case II we develop a new analytical model for the growth of composite solid; the model approximates the solid/melt interface as being flat. Its predictions are compared with the results of several laboratory experiments in which a supereutectic melt was cooled and solidified from below.

3. Case I: subeutectic melt cooled from below

When a subeutectic melt is cooled from below, with the cooling boundary maintained below the eutectic temperature, then if the solid/melt interface is approximately flat it remains at eutectic temperature, and the melt just above this interface has eutectic composition. Therefore the variation with depth of both the temperature and the composition in the melt produce a gravitationally stable density field. There will be no convective motions in the melt and diffusion is the only transport mechanism available in the melt for the fluxes of solute and heat.

When the far-field conditions in the melt are fixed, and the boundary conditions described above are applied, there is a similarity solution governing the morphologically stable, flat-interface growth (Worster 1983). This predicts that the solid composition takes a fixed value between that of pure component A and the far-field

composition in the melt. The solid becomes compositionally stratified only if the far-field conditions are allowed to vary.

If a mush phase develops, we can modify the mush model of Worster (1986) so that the solid/mush interface temperature is eutectic and the base is at a temperature below eutectic. At the solid/mush interface, composite eutectic solid forms in the interstices between the dendritic crystals of pure solid A. The equations governing the solidification are given in Worster (1986) and admit a similarity solution if the far-field conditions are fixed. In this solution, the solid composition and the solid fraction at the solid/mush boundary are fixed in time. Therefore, as in the morphologically stable case, the solid has a fixed bulk composition, at all depths, until the far-field conditions change. We deduce that no compositional stratification occurs in diffusively grown solid, until the influence of the boundaries of the container is important.

4. Case II: supereutectic melt cooled from below

4.1. *Introduction*

If a supereutectic melt is cooled from below, again with the cooling boundary set below eutectic temperature, then, at thermodynamic equilibrium, the solid/melt interface temperature is eutectic and the composition of the melt at the interface is eutectic. There is now a stabilizing temperature field and a destabilizing compositional field in the melt. We assume that the increase of density with composition is much greater than the decrease with temperature, as discussed in §2.2. The compositional destabilization will dominate the thermal stabilization and for sufficiently large Rayleigh numbers, compositionally driven convection will occur. When the compositional Rayleigh number is very large this convection becomes very vigorous and mixes the melt uniformly (Krishnamurti 1970). Following the terminology given by Turner (1979), we describe this type of convection as 'turbulent'. In typical laboratory conditions the compositional Rayleigh number is of the order of 10^{11}, and so the convection can be considered to be turbulent and generate a well-mixed melt. We note that in the laboratory experiments, to be described below, the compositionally depleted fluid, which rose from the basal boundary layer, mixed into the surrounding fluid and did not pool at the top of the tank. This mixing is effected by a combination of the development of shear instabilities in the rising plumes of depleted fluid and the lateral diffusion of composition before the plumes have travelled the extent of the tank. Figure 3 shows a shadowgraph of this compositional convection during a typical experimental run.

In the present theoretical model, we consider the properties of the system averaged over several crystal widths, so that the horizontal variations on the scale of individual crystals in the thermal and compositional fields due to the composite nature of the solid do not complicate the problem (Elliott 1983). Further, we make the simplifying approximation that the solid/melt interface is flat. In practice, the interface will only be flat for a very small range of melt compositions about the eutectic (as discussed in §2.4) and beyond this range the interface will be mushy. In the experimental observations, described in §5, however, a mush layer of about 1 mm thickness formed and so this approximation is quite reasonable for this first-order model. We compare our theoretical model (§4.4) with experiments (§5) in which such composite solid was grown, and obtain good agreement. The problem is

FIGURE 3. Shadowgraph of the compositionally driven convection during an experimental run.

much more complex when an intermediate mush phase is included; Fowler (1985) described a preliminary study of this problem and we are currently investigating a more detailed model of the solidification which includes an intermediate mush zone.

A simple model of the flat-interface solidification process has been proposed by Kerr (1984). In his model, the cooling boundary was maintained above eutectic temperature and solid of pure component B (figure 1) was grown. His model constrained the melt to lie on the liquidus and he specified the solid/melt interface temperature to be the same as that of the melt interior. He determined the rate of cooling of the melt and the growth rate of the solid layer using a simple global balance of energy and composition. Because of these simplifications, details of the compositional and thermal fluxes at the solid/melt interface did not need to be considered. However, such details are necessary to predict the solid composition when the cooling boundary is below the eutectic temperature. Therefore, we relax the boundary conditions that were imposed in his simple global theory and address the form of the boundary layers above the interface.

4.2. *The compositional flux*

The compositional flux at the solid/melt interface of a melt in turbulent compositional convection is analogous to the thermal flux at the cooled/heated boundary of a fluid in turbulent thermal convection. In the thermal case, the motion is generated by heating from below or cooling from above, and the thermal flux may be considered independent of the depth of the fluid layer. Therefore the thermal Nusselt number, Nu, is given by $Nu = K_T Ra^{\frac{1}{3}}$, where K_T is an empirically determined constant, and Ra is the thermal Rayleigh number. The temperature variations are confined to thin boundary layers near the horizontal boundaries, with an

approximately uniform melt temperature in between. The heat transfer across these thermal boundary layers is

$$F_T = K_T \left(\frac{g\alpha \Delta T}{\kappa_m \nu} \right)^{\frac{1}{3}} k_m \Delta T, \tag{4.1}$$

where κ_m is the melt thermal diffusivity, ν the kinematic viscosity, α the coefficient of thermal expansion and ΔT is the temperature jump across the thermal boundary layer.

The analogous result for the compositional flux in compositionally driven convection is

$$F_C = K_C \left(\frac{g\beta \Delta C}{D\nu} \right)^{\frac{1}{3}} D \Delta C, \tag{4.2}$$

where D is the compositional diffusivity, β is the fractional increase in melt density per unit increase in composition (cf. α) and K_C is an empirically determined constant, which may be different from K_T because there is no compositional flux across the upper boundary of the melt, in contrast to the analogous thermal convection problem in which there is a heat transfer across both boundaries.

4.3. *The thermal flux*

When determining the heat transfer from the melt across the compositional boundary layer and into the solid, two distinct situations need to be considered; in an undersaturated melt the temperature and composition of the melt can evolve independently, while in a saturated melt the temperature is constrained to follow the evolution of the composition along the liquidus, as shown in figure 4.

4.3.1. *Undersaturated melt*

When the melt is undersaturated three possible descriptions of the mechanism of heat transfer can be envisaged. These are briefly outlined below; the main difference in the models is the dependence of the ratio of the thermal flux to the compositional flux on the ratio κ_m/D. In most situations $\kappa_m/D \gg 1$. In the laboratory experiments (§5), the compositional convection manifested itself as thin plumes of light fluid rising from the compositional boundary layer, with a compensating net downflow from the melt (figure 3) and we note here that models II and III (see below) best describe these results.

Model I: thermal diffusion across the compositional boundary layer. If the compositional convection is sufficiently vigorous it will mix the melt above the compositional boundary layer to a uniform temperature and composition. The temperature decrease between that in the far-field melt and the eutectic now occurs across the compositional boundary layer. This boundary layer has a thickness $(D\Delta C/F_C)$ and so the thermal flux will be of the form

$$F_T = \mu \rho_m c_m \left(\frac{\kappa_m \Delta T}{D\Delta C} \right) F_C, \tag{4.3}$$

where μ is a constant of order 1, ρ_m is the melt density and c_m is the specific heat of the melt.

Model I is equivalent to the statement that as the cold light fluid rises through the compositional boundary layer, its temperature increases to that of the far field. This model predicts a very large heat transfer given the nature of the convection and the difference in the diffusivity of composition and temperature (κ_m/D).

Model II: thermal advection balancing thermal diffusion. If the convection-driven

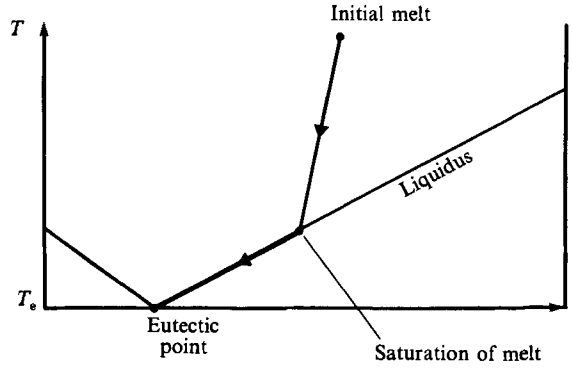

FIGURE 4. Evolution of melt in the phase diagram, showing the discontinuity in rate of change of temperature with concentration.

mixing is not efficient, parcels of compositionally buoyant, but cold, fluid can rise out of the compositional boundary layer and into the melt above, before their temperature has adjusted to the far-field ambient temperature. By continuity, there is a compensating mean downflow of warmer heavy fluid. Away from the neighbourhood of one of the upward-rising, compositionally buoyant parcels the temperature will adjust from the interface temperature to the far-field temperature over a length determined by a vertical thermal advection/diffusion balance for this mean downflow. The appropriate thermal lengthscale includes the melt thermal diffusivity κ_m and the mean vertical velocity towards the boundary layer, v, and so is κ_m/v. The velocity v is determined by the compositional flux, $v \sim F_C/\Delta C$. This gives the effective thermal boundary-layer thickness $\delta T \sim \kappa_m \Delta C/F_C$. Therefore the thermal flux into the boundary layer is of the form

$$F_T = \mu \rho_m c_m \left(\frac{\Delta T}{\Delta C}\right) F_C, \tag{4.4}$$

where μ is an empirically determinable constant.

This model constrains the thermal flux to be rate-limited by the mean compositionally driven velocity field. In practice the heat transfer from an undersaturated melt may be greater than this because the light field rises in a series of narrow plumes, with lateral as well as vertical thermal diffusion. Howard (1964) introduced a simple mechanism for convection of a single-component fluid at high Rayleigh number based on the description of thermals breaking away from a diffusing boundary layer. In the present situation, we have a high Rayleigh number, double-diffusive interface in which the slower diffusing component (here the composition) is unstable. In model III, we adopt an approach similar to that of Howard (1964) to describe both the thermal and compositional boundary layers and then deduce an expression for the thermal flux in terms of the compositional flux.

Model III: thermal diffusion balancing periodic sweeping of the boundary layer. We consider modelling the heat transfer from the melt when the buoyant fluid rises from the solid/melt interface as a series of pulses which are discrete in both space and time. Between successive pulses, which sweep away the fluid from just above the interface, diffusive compositional and thermal boundary layers develop. If t is the time elapsed since the previous sweeping motion, the thermal boundary layer will be of thickness

$(\kappa_m t)^{\frac{1}{2}}$ and the compositional boundary layer of thickness $(Dt)^{\frac{1}{2}}$. Thus, taking the spatial and temporal average, the mean thermal boundary layer is of thickness $(\kappa_m/D)^{\frac{1}{2}}$ times that of the compositional boundary layer. This gives a thermal flux of the form

$$F_T = \mu \rho_m c_m \left(\frac{\Delta T}{\Delta C}\right)\left(\frac{\kappa_m}{D}\right)^{\frac{1}{2}} F_C, \tag{4.5}$$

where μ is an empirically determinable constant.

In model III the effective thermal boundary-layer thickness is smaller than that of model II and so it predicts a greater heat transfer from the melt. However, because it incorporates the difference between thermal and compositional diffusivities in determining the boundary-layer thicknesses, it predicts a smaller heat transfer than model I. This difference in diffusivities is important when the convective mixing is not highly efficient.

4.3.2. *Saturation*

In the models of the heat transfer described above, the temperature and composition of the melt are assumed to evolve independently. However, when the melt becomes saturated, the constraint of thermodynamic equilibrium requires the temperature to follow the composition along the liquidus. Therefore, in a saturated melt, the thermal flux is given directly in terms of the compositional flux

$$F_T = \rho_m c_m m F_C, \tag{4.6}$$

where m is the linear liquidus slope $\Delta T/\Delta C$. In the experiments, described in §5, some degree of melt supersaturation was observed; this is not possible in the equilibrium model but we consider this in more detail in §5.

4.4 *The mathematical model*

The solidification may be described quantitatively by the following equations which represent the compositional and thermal flux balances in the melt and at the solid/melt interface. We incorporate the approximation that the solid/melt interface is flat (on a scale greater than the crystal scale). Strictly, this is valid only when the melt composition is close to eutectic and composite eutectic solid forms, but comparison with experiments (§5) indicates that it is a good approximation if the mush layer is thin (of order 1 mm). The liquidus slope m is taken to be a constant. A schematic of the solid/melt configuration for this model is shown in figure 5.

At the solid/melt interface, the thermal balance has the form

$$\rho_m c_m \dot{h}(T_m - T_e) + \rho_s L\dot{h} + \rho_m c_m h_C A(T_m - T_e)(C_m - C_e)^{\frac{1}{3}} = k_s \frac{(T_e - T_b)}{h}, \tag{4.7a}$$

where ρ_m and ρ_s are the melt and solid densities, h is the solid thickness, L the specific latent heat of fusion and $h_C = K_C(g\beta/Dv)^{\frac{1}{3}}D$. We have introduced the parameter A to represent the ratio of the thermal to compositional flux at the solid/melt interface. We have assumed that the temperature profile in the solid is linear, which is a good approximation to the solution of the full diffusion equation provided that the solid growth is slow. At the solid/melt interface the compositional flux satisfies

$$\dot{h}(C_s - C_m) = h_C(C_m - C_e)^{\frac{4}{3}}, \tag{4.7b}$$

where C_s is the composition of the solid. The cooling of the melt is given by

$$\rho_m c_m (H - h)\dot{T}_m = -\rho_m c_m h_C A(T_m - T_e)(C_m - C_e)^{\frac{1}{3}}, \tag{4.7c}$$

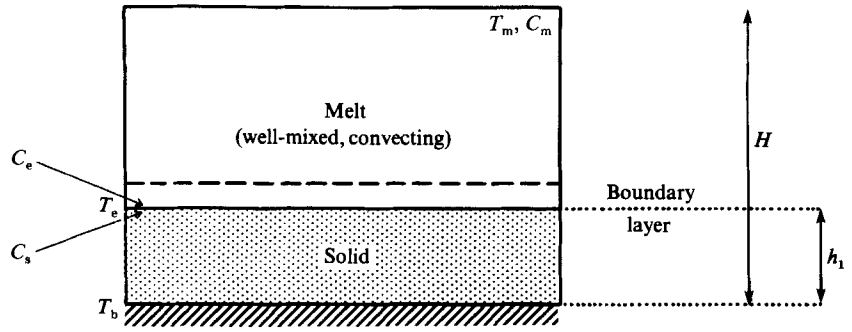

FIGURE 5. Geometry of the one-dimensional flat-interface solidification model discussed in §4.

where H is the initial depth of the melt layer, and the composition of the melt decreases according to the equation

$$(H-h)\,\dot{C}_m = -h_C(C_m-C_e)^{\frac{4}{3}}. \tag{4.7d}$$

To simplify these questions we introduce the non-dimensional parameters ψ, θ, ϕ, τ, and $\hat{h}$ given by

$$C_m = C_0+\psi(C_e-C_0),$$
$$T_m = T_0+\theta(T_e-T_0),$$
$$C_s = C_0+\phi(C_e-C_0),$$
$$t = \frac{\tau}{\alpha}, \quad \text{where} \quad \alpha = \frac{h_C(C_0-C_e)^{\frac{1}{3}}}{H},$$
$$h = H\hat{h}.$$

These give rise to the non-dimensionalized equations (dropping the caret on h),

$$\dot{h}(1-\theta+S)+A(1-\theta)(1-\psi)^{\frac{1}{3}} = \frac{\gamma}{h}, \quad (1-h)\,\dot{\psi} = (1-\psi)^{\frac{4}{3}}, \tag{4.8a,b}$$

$$(\psi-\phi)\,\dot{h} = (1-\psi)^{\frac{4}{3}}, \quad (1-h)\,\dot{\theta} = A(1-\theta)(1-\psi)^{\frac{1}{3}}, \tag{4.8c,d}$$

where the non-dimensional number

$$\gamma = \left(\frac{k_s(T_e-T_b)}{h_C H(T_0-T_e)(C_0-C_e)^{\frac{1}{3}}}\right)\left(\frac{1}{\rho_m c_m}\right)$$

is a measure of the ratio of the heat transfer across the solid to the heat transfer from the melt, and the Stefan number,

$$S = \frac{\rho_s L}{\rho_m c_m (T_0-T_e)}.$$

The initial conditions take the non-dimensional form

$$\phi = \theta = \psi = h = 0 \quad \text{at} \quad \tau = 0. \tag{4.8e}$$

For a typical experiment using sodium carbonate (§5) the above parameters have the values given in table 1 (*a*).

The above model is valid after the initial quenching phase during which time the growth of solid is constrained by the crystal nucleation kinetics. However, it is

(*a*) Values for the laboratory experiment with an aqueous Na_2CO_3 solution. The data have been collected from a variety of sources including Weast (1971), Huppert & Worster (1985) and Turner *et al.* (1986).

$\kappa_m = 1.3 \times 10^{-3}$ cm^2 s^{-1} $\quad D = 10^{-5}$ cm^2 s^{-1}
$\kappa_s = 8.9 \times 10^{-3}$ cm^2 s^{-1} $\quad g = 10^3$ cm s^{-2}
$c_m = 3.9 \times 10^3$ J kg °C^{-1} $\quad \beta = 10^{-2}$
$c_s = 1.9 \times 10^3$ J kg °C^{-1}
$\nu = 2.3 \times 10^{-2}$ cm^2 s^{-1} $\quad T_e = -2.1$ °C
$L = 3.0 \times 10^5$ J kg^{-1} $\quad T_0 = 18.4$ °C
$T_b = -20$ °C $\quad C_0 = 9.37\%$
$C_e = 5.97\%$ $\quad H = 22$ cm

$$S = \left(\frac{\rho_s L}{\rho_m c_m (T_0 - T_e)}\right) = 3.55 \qquad \rho_m = 1070 \text{ kg m}^{-3}$$

$$\alpha = \frac{1}{H} h_C (\Delta C)^{\frac{1}{3}} = 2.40 \times 10^{-4} K_C \text{ s}^{-1} \qquad \rho_s = 1012 \text{ kg m}^{-3}$$

$$h_C = K_C \left(\frac{g\beta}{D\nu}\right)^{\frac{1}{3}} D = 3.52 \times 10^{-3} K_C \text{ cm s}^{-1}$$

$$\gamma = \frac{k_s}{\rho_m c_m h_C} \frac{(T_e - T_b)}{H(T_0 - T_e)(C_0 - C_e)^{\frac{1}{3}}} = 3.08 \times 10^{-2} K_C^{-1}$$

Empirical results indicate that $\gamma \approx 0.2$, and so $K_C \approx 0.15$.

(*b*) Values for a Komatiite lava (from Turner *et al.* 1986)

$\kappa_m = 5.0 \times 10^{-3}$ cm^2 s^{-1} $\quad D = 10^{-9}$ cm^2 s^{-1}
$\kappa_s = 5.0 \times 10^{-3}$ cm^2 s^{-1} $\quad g = 10^3$ cm s^{-2}
$c_s = c_m = 7.3 \times 10^2$ J kg^{-1} °C^{-1} $\quad \beta = 10^{-6}$
$\nu = 2.0$ cm^2 s^{-1} $\quad T_e = 1400$ °C
$L = 5.0 \times 10^5$ J kg^{-1} $\quad T_0 = 1600$ °C
$T_b = 1200$ °C $\quad C_0 = 10\%$
$C_e = 15\%$ $\quad H = 10^5$ cm
$S = 3.42$
$\alpha = 2.0 \times 10^{-13}$ s^{-1}
$h_C = 1.19 \times 10^{-8}$ cm s^{-1}
$\gamma = 2.46$ using $K_C = 0.15$.

TABLE 1. Parameter values

estimated from experimental observations that within a few minutes the nucleation kinetics are not important, and thus we ignore this effect here.

4.5. *Asymptotic solutions of the full equations*

Asymptotic solutions of (4.8) for small and large times have been obtained in the cases $A \gg 1$ and $A \sim 1$ and are given in the Appendix. In the analysis for $A \gg 1$, the thermal equilibrium assumption (§4.3) is not imposed and the melt is predicted to become supersaturated; in order to incorporate the equilibrium constraint, (4.6) (corresponding to $A = 1$) should be applied when the melt becomes saturated. When $A \gg 1$, the asymptotic analysis reveals four growth regimes, which hold at different times during the solidification. When $A = 1$, only the first and last of these regimes occur. We now discuss the physical balances involved in each of these four regimes. Note that the first three regimes may be identified in the numerical solution of the full equations shown in figure 6. From this solution it is seen that the two main regions of significant compositional change occur in regimes 1 and 4.

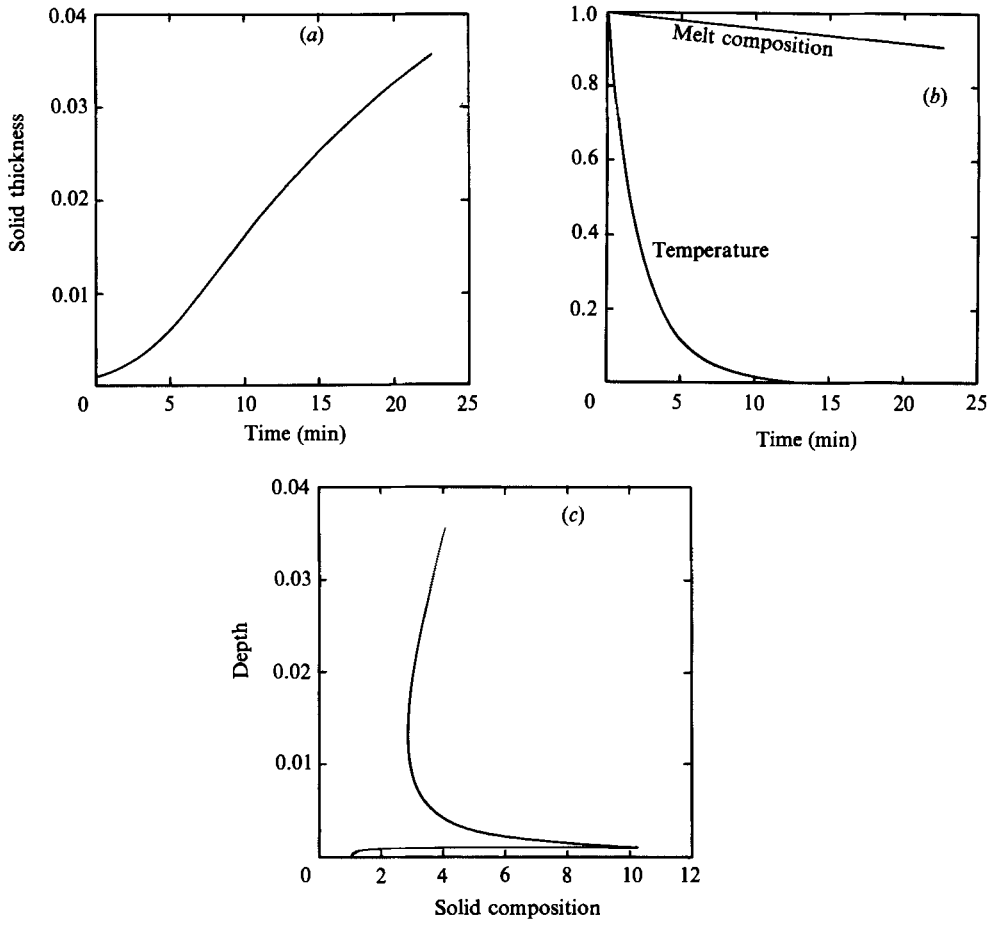

FIGURE 6. $S = 10$, $\gamma = 0.1$, $A = 100$. (*a*) Thickness of the solid layer, $\hat{h}$, as a function of time. (*b*) Evolution of the temperature, $1-\theta$, and composition, $1-\psi$, in the melt with time. (*c*) Solid composition, $1-\theta$, as a function of depth in the solid, $\hat{h}$.

When the solid first begins to form on the cold boundary, it grows very quickly so that the rate of production of enthalpy of fusion is sufficient to balance the large heat transfer across the thin solid layer. The heat transfer from the melt is not important in the energy balance. This is regime 1. Initially the solid will have the same composition as the melt. However, the conductive thermal flux across the solid layer decreases as the layer grows. As a result, less latent heat of fusion is required to balance the heat transfer across the solid and the growth rate of the solid decreases. During the process, the compositional flux is approximately constant because the solid layer remains relatively thin. Therefore, with time, a greater quantity of solid of composition B is deposited in the composite solid, thus increasing its composition. This growth regime persists until the convective heat flux from the melt balances the conductive heat flux into the solid, and the rate of production of latent heat of fusion is not important in the thermal energy budget. This is regime 2. As the melt cools, the growth rate now increases to reduce the conductive thermal flux through the solid. This increase in the growth rate causes a decrease in the composition of the solid that is formed. When the melt has cooled sufficiently, the latent heat of fusion produced during the solidification again becomes important and balances the

conductive heat transfer across the solid. This is regime 3. The growth rate now decreases and the solid composition increases, as in regime 1. Regime 3 applies until the rate of decrease of the composition of the melt exceeds the decrease in the solid rate (§4.3.2). This occurs when a sufficiently large quantity of solid has formed. At this stage, the fourth asymptotic regime applies in which the solid composition decreases towards eutectic, and total solidification of the melt follows.

In summary, the two main mechanisms generating solid stratification are the variation in the solid growth rate and the decay of the ambient composition.

When $A = 1$, the melt is predicted to cool down to eutectic temperature at the same rate as its composition falls to eutectic composition. Therefore, the solution for small times, in which the composition of the solid deposited increases with time (cf. regime 1), merges directly into the solution in which the compositional decay in the ambient melt causes the solid composition to decrease (cf. regime 4). Such a compositional profile may be identified in the numerical results shown in figure 7 for which $A = 2$.

The equilibrium constraint

If the equilibrium constraint is imposed by applying (4.6) (i.e. $A = 1$) when the melt becomes saturated then the solid can exhibit either all four of the regimes which are present in the case $A \gg 1$ or just the two regimes that occur when $A = 1$ described above. This depends upon the value of A and the initial degree of undersaturation and can be seen in the numerical solutions of the equations (for example figures 11 and 12). The asymptotic solutions given for $A = 1$ and $A \gg 1$ may be combined to predict the growth when the equilibrium constraint is imposed.

4.6. *Comparison of the predictions of the thermal flux models*

The difference in the thermal models may be seen by comparing the different predictions of the rate of cooling of the melt relative to the rate of decrease of its composition. Equations 4.8(b, d) may be combined to give the relationship between the composition and the temperature of the melt:

$$(1-\theta) = (1-\psi)^A. \tag{4.9}$$

Equation (4.9) has been plotted for the values $A = 1$, 2, 3, 10, 100 on figure 8, together with a typical liquidus (dotted line). This shows the degree of supersaturation predicted by each of the values of A if the equilibrium constraint is not imposed when the melt becomes saturated. These curves may be compared with some experimental data (shown as plus signs) which are described later. With the equilibrium constraint imposed, the value of A is changed to 1 when the melt becomes saturated and the melt then follows the liquidus. This is a thermodynamical constraint rather than a fluid-dynamical constraint.

If the melt is initially undersaturated, the temperature of the melt is expected to decrease more rapidly than the composition. Therefore, the melt will become saturated, which indicates that models I or III, which correspond to $A > 1$, are the most applicable for an undersaturated melt. As a first approximation, we would expect the value of A to be independent of the degree of undersaturation, because the convection is turbulent.

In models II and III the thermal boundary layer is thicker than the compositional boundary layer. Therefore some of the melt in the thermal boundary layer may be supersaturated even if the melt is undersaturated in the far field. Such supersaturation may admit interfacial instability, with the formation of a mush (§2.3).

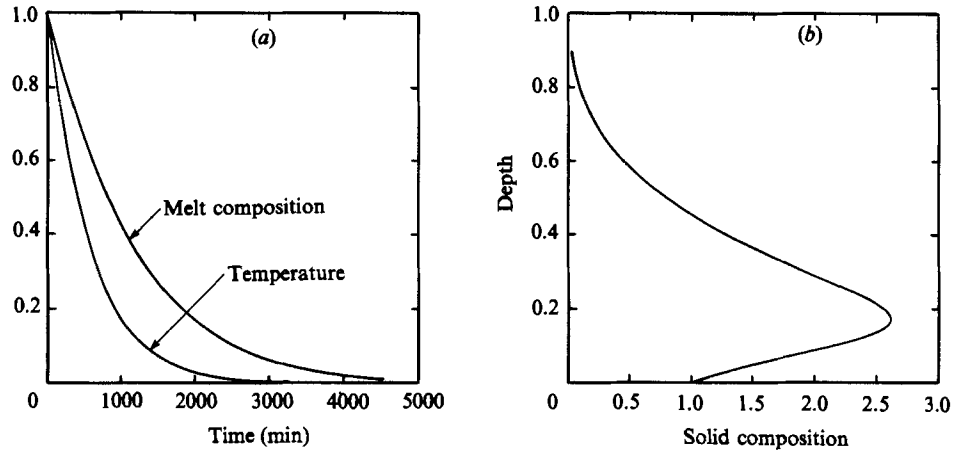

FIGURE 7. $S = 4.25$, $\gamma = 0.56$, $A = 2$. (*a*) Evolution of the temperature, $1-\theta$, and composition, $1-\psi$, in the melt with time, t, in min. (*b*) Variation of solid composition, $1-\phi$, with depth in the solid, $\hat{h}$.

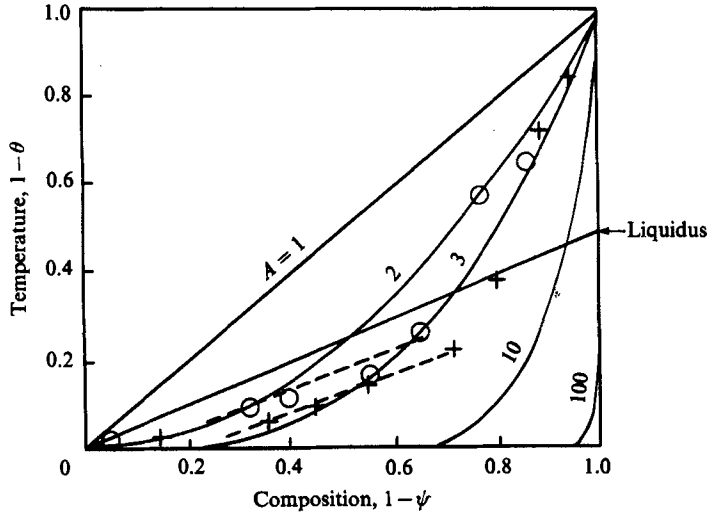

FIGURE 8. Plot of temperature, $1-\theta$, against composition, $1-\psi$, in the melt, as it evolves in time. Curves given for the parameter $A = 1, 2, 3, 10, 100$ in (4.9). Experimental data are marked by + and ○ for two different experiments using aqueous Na_2CO_3.

For typical experimental conditions, the morphological stability criterion of Hurle & Jakeman (1968) (§2.4) does not hold. Although we cannot apply this criterion quantitatively because it ignores the effect of the melt convection, we might expect a mush phase to develop. The observations indicate that this mush is thin (approximately 1 mm) and that as the experiment proceeds the mush becomes thinner. Thus it should not significantly change the nature of the solid stratification that would develop with a flat interface.

The next section describes some laboratory experiments in which a supereutectic melt was cooled from below. These have been performed to establish the accuracy of the equilibrium model for the growth of composite solid. A value for A may then be

estimated and the most appropriate thermal-flux model of §4.3 can be determined. These experiments also enable an estimate for the constant K_C in the compositional flux law to be determined.

5. Laboratory experiments

Several laboratory experiments have been performed in which a supereutectic aqueous solution of sodium carbonate was cooled from below at a temperature below the eutectic. The apparatus used is described in Huppert & Worster (1985) and Kerr (1984). In brief, it consists of a Perspex rectangular tank, $20 \times 20 \times 40$ cm, with a basal cooling plate through which a coolant is circulated. When a solid layer of thickness 10–15 cm had formed from the melt, the solid was removed and a vertically cored sample taken. This was divided into equal lengths, and the composition of each piece was measured, by a hand-held refractometer, to determine the variation with depth of the composition in the solid.

5.1. *General features*

We now describe the important features observed in a typical experimental run. At the beginning of the experiment, it was difficult to maintain the temperature of the fluid in the cooling plate at a fixed temperature, well below the eutectic, since it was not pumped through the cooling plate sufficiently fast. Also, the initiation of nucleation was not immediate. However, after about an hour a constant basal-plate temperature was attained and a fine layer of crystals had formed on the base of the tank. Fairly strong compositional convection was generated in the melt by this growth. This was observed using a shadowgraph. A few crystals then began to grow in the plane sheets protruding from the solid/melt interface at various angles to the vertical. These crystals were of pure component B ($Na_2CO_3 \cdot 10H_2O$) and extended through a depth of at most 2 cm. From the experimental observations they appeared to be very sparsely distributed and although their number density increased with time, it was always small. On close inspection, the main solid/melt interface, below these crystals, had an uneven surface, with many small dendrite-like crystals protruding approximately 1–2 mm from the purely solid layer. It is this thin mush-type zone which was approximated as being flat in the model of §4, and the sparsely distributed sheet-like crystals are not accounted for in the theory. As the mush developed, the convection in the melt became very vigorous and extended throughout the melt.

After about 12 hours the solid layer, now about 3 cm thick had enveloped all of the protruding sheet-like crystals and for the remainder of the experiment the interface between the solid and the melt just had a very thin mush-type structure, estimated to be of the order of 1 mm thick. The approximation of a flat interface in the preceding theory describes the subsequent solidification quite accurately. Towards the end of the experiment, the convection decayed as the melt composition tended towards eutectic and the transport in the melt became diffusively governed.

5.2. *Experimental results*

5.2.1. *Melt evolution*

During the experiments, measurements were made of the concentration and temperature at various depths in the melt; these confirmed the hypothesis that the ambient melt was well mixed and uniform (figure 3). Figure 9 shows the temperatures at 3 different depths in the melt during a typical experiment. The lower thermistor

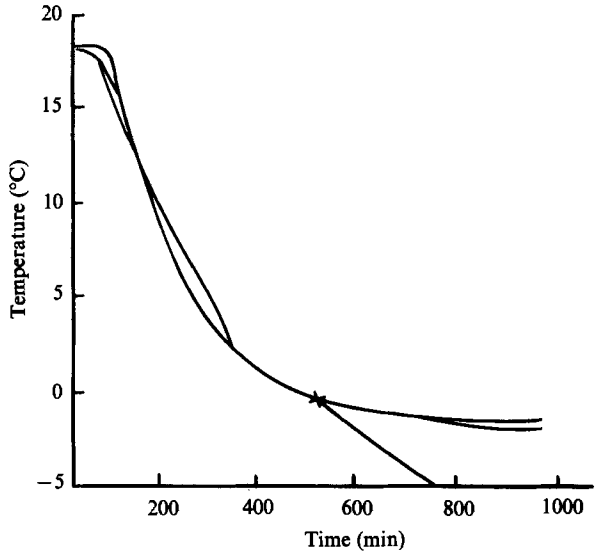

FIGURE 9. Experimental measurements of the melt temperature at three depths in the melt.

became frozen into the solid phase after the point marked with a cross. The evolution of the depth-averaged melt temperature with concentration is shown in non-dimensional form in figure 8 for two experiments (marked with crosses and circles). This suggests that when the melt is undersaturated the temperature decays faster than the composition, as anticipated (§4.2). Also it predicts that a significant degree of supersaturation is attained before the compositional control of the temperature becomes effective. The undersaturated melt evolution may be reproduced theoretically using the approximate value $A = 3$ in the preceding theory (figure 8). The experimental results also show that on reaching some degree of supersaturation, the temperature follows the evolution of the composition, on a line approximately parallel to the liquidus. We deduce that the thermal flux is now constrained by the compositional flux with $A = 1$, and conclude that equilibrium effects are important. The supersaturation possibly represents surface energy effects; we regard this simply as lowering the liquidus.

An estimate for the value of γ and a further estimate of A may be obtained from the gradients of plots of $\log(1-\theta)$ and $\log(1-\psi)$ as functions of time for the experimental data. These gradients are compared with those of the asymptotic solutions which apply when the melt is undersaturated. We have

$$(1-\theta) \sim \mathrm{e}^{-A\tau}, \tag{5.1}$$

and

$$(1-\psi) \sim \mathrm{e}^{-\tau}. \tag{5.2}$$

This comparison gives the estimates $A \approx 3$ and $\gamma \approx 0.2$. Note that this second estimate of A agrees closely with that obtained earlier. Figure 10 shows the predicted evolution of (*a*) θ and ψ, and (*b*) the solid thickness with time using these parameter values compared with the evolution measured in the laboratory (circles and crosses).

5.2.2. *The solid composition*

The measurements of the solid composition are shown on figure 11. The composition varies with thickness in a fashion similar to that predicted by the model

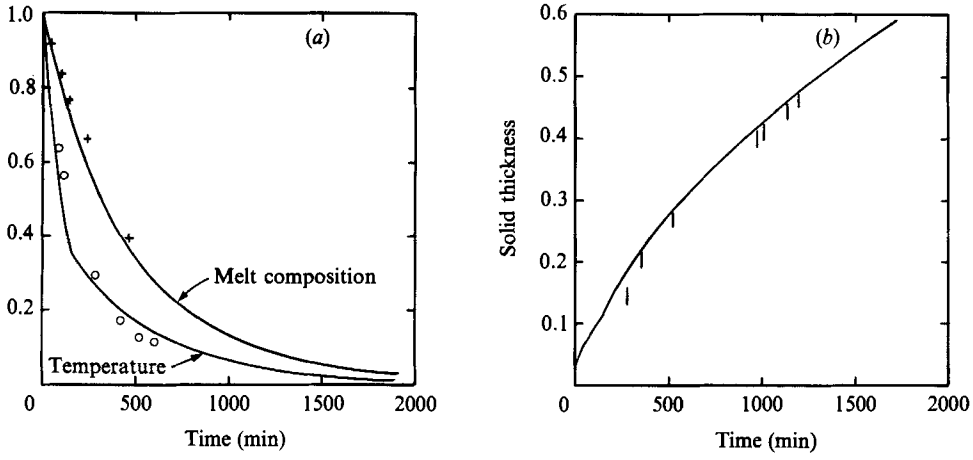

FIGURE 10. (*a*) Measured evolution of the melt temperature, $1-\theta$, (○) and composition, $1-\psi$ (+) with time, and the corresponding prediction of the equilibrium model of §4, with $A = 3$, $S = 3.55$ and $\gamma = 0.2$. (*b*) The thickness of the solid layer, $\hat{h}$, as a function of time, t, in min as measured experimentally (|) and as predicted by the theory with the parameters of (*a*).

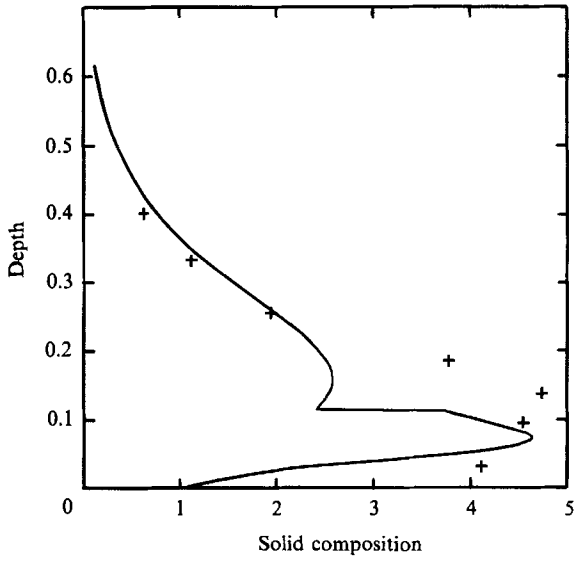

FIGURE 11. Variation of the solid composition, $1-\phi$, as measured (+) in a block solidified from aqueous Na_2CO_3 and as predicted by the equilibrium model with $A = 3$, $\gamma = 0.2$ and $S = 3.55$. Note the discontinuity in the theoretical prediction of the composition gradient caused by the equilibrium constraint.

of §4.4 with $A = 3$ for the undersaturated melt, $A = 1$ when saturated, and $\gamma = 0.2$ (shown as the solid line). However there is some difference between the model solution and the laboratory measurements during the early part of the experiment. The experimentally observed compositions in the lower 2 cm of the solid are somewhat larger than those predicted by the model using the parameter values given above and do not change as rapidly with depth near the point of maximum composition as predicted by the flat-interface theory. This is interpreted as being a consequence of the development of the thin mush phase; the effect is amplified

because of the local vertical averaging involved in the measurements. The development of mush may also result in the composition further up the solid being lower than predicted theoretically. To maintain equilibrium on saturation of the melt, the value of A is changed to $A = 1$; this produces a discontinuity in the theoretically predicted compositional gradient of the solid (figure 11). However, in practice, supersaturation effects in conjunction with the mush will act to make the solid gradient more continuous.

In summary, the experiments indicate that the thermal flux appears to have two different forms according as the melt is undersaturated or saturated. When undersaturated, the value of A is approximately 3 and the melt cools to become saturated (figure 8). On reaching a certain degree of supersaturation, the thermal flux becomes constrained by equilibrium effects and the melt evolves along a line close and approximately parallel to the liquidus. At this point, A takes the value $A = 1$, ignoring the supersaturation. We deduce that in an undersaturated melt, the intermittent, compositionally driven sweeping motions balancing the thermal diffusion, suggested in model III, work to increase the heat transfer from the melt predicted by the advection/diffusion balance of model II. However, in a saturated melt, the evolution of the temperature is thermodynamically constrained to follow the evolution of the composition along the liquidus. The flat-interface solid model predicts the solid composition reasonably accurately and the error due to ignoring the formation of the mush is not too great.

6. Application to magma chambers

The model proposed here may be used to predict the extent of the stratification in the base of a solidified magma chamber. We apply the model to an idealized solidifying magma chamber. We assume that there is efficient hydrothermal cooling outside the chamber which maintains the roof, base and sidewalls at constant temperature. Further, we assume that when a large body of molten magma is deposited in the chamber, the solid that initially forms at the base of the chamber is produced by local cooling. This is not necessarily true at a later stage, when solid may form at the base owing to cooling elsewhere (Turner, Huppert & Sparks 1986).

Figure 12 shows the predicted stratification generated by this process, up to the point at which one half the material in the chamber has solidified on the base. The figure was calculated using parameter values appropriate for a magma, shown in table 1(*b*), in conjunction with the equilibrium model of §4.5. The figure indicates that the composition of a typical heavy element in the magma may increase by over 40% of its initial composition above eutectic in the lower 300 m of a 1 km deep chamber, with a reversal in the compositional gradient above this region. (The magma is treated as a binary melt with the typical heavy element as the component B in the model of §4.) This could be a significant result in the interpretation of geological data; for example, the layering in the Skaergaard intrusion (McBirney & Noyes 1979). The model may be used qualitatively to understand the initial solidification on the base. We note that in a real situation the basal solid may be contaminated by solids formed at the roof and sidewalls of the chamber which fall onto the floor. Also, the model ignores the cooling of the melt through the sidewalls, and the resulting change in the convection and composition of the melt. Some of the effects of sidewall cooling have been considered by Adornato & Brown (1987). However, these effects should not significantly affect the nature of the composition near the chamber floor.

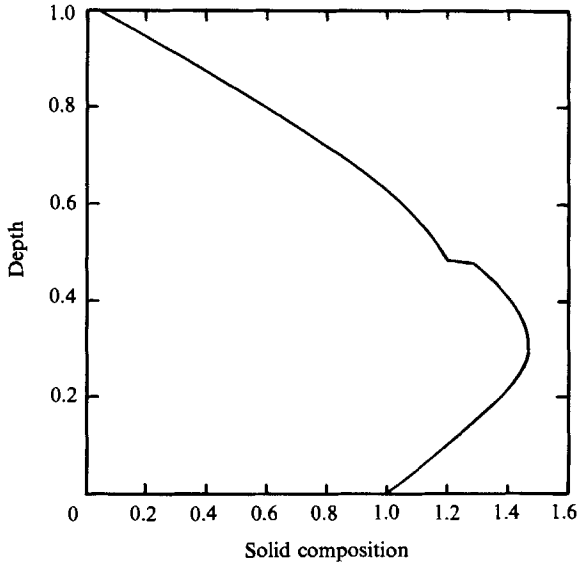

FIGURE 12. Predicted variation of a heavy component, $1-\phi$, with depth, $\hat{h}$, in a magma chamber which has solidified from below. Here $\gamma = 2.46$, $S = 3.42$ and $A = 3$.

7. Conclusions

The compositional stratification produced in composite solid grown from a binary melt on a lower cooling plate of fixed temperature depends upon whether the melt composition is sub- or supereutectic. In both cases, the solid/melt interface must be at the eutectic temperature in order to grow composite solid.

In a subeutectic melt, a similarity solution for the diffusion-governed growth holds until the far-field conditions change. In this solution, the solid has a fixed composition, irrespectively of whether an intermediate mush phase forms during the solidification. When the far-field conditions change, global conservation of solute requires the solid composition to change.

In a supereutectic melt, compositionally depleted, and therefore light, fluid is released at the solid/melt interface; this generates vigorous convection in the melt which changes the heat and mass transfer across the solid/melt interface. In the present study we have derived a model of this solidification process in which the solid/melt interface is approximated as being flat. The solid composition is predicted to increase initially as the solid growth rate decreases, but subsequently to decrease when the solid layer is thicker and the composition of the melt decreases. Laboratory experiments with an aqueous solution of sodium carbonate confirmed these predictions, and indicated that the solid/melt interface consists of a mush phase, approximately 1 mm thick. The laboratory results are consistent with the flux laws $F_C = \lambda(\Delta C)^{\frac{4}{3}}$ and $F_T = A\rho_m c_m \lambda(\Delta C)^{\frac{1}{3}}(\Delta T)$ for compositionally driven turbulent natural convection, with a stabilizing temperature field. The parameters λ and A have been estimated empirically as $\lambda = 0.15D(g\beta/D\nu)^{\frac{1}{3}}$, and $A = 3$ for an undersaturated melt and $A = 1$ for a saturated melt of aqueous sodium carbonate.

Weaknesses in the present theory include the neglect of supersaturation effects, observed in the laboratory, and the simplifying approximation of a flat solid/melt interface. We are presently investigating the incorporation of a mush phase in the solidification model and it will be interesting to compare the results of the present

study with the more complex model. It would seem from the analysis of this study that a similar compositional profile will develop when solid forms behind a mush phase. The present composite eutectic model gives a first approximation to the form of the solid stratification possible.

Paul Bruce, Ross Kerr, John Lister and Grae Worster contributed to the understanding of the physical processes involved in the problems considered in this work, through many discussions and some assistance with the laboratory experiments. Useful comments from Don Hurle on an earlier version of the manuscript are gratefully acknowledged. Our work is supported by grants from the BP Venture Research Unit, the NERC and St John's College, Cambridge.

Appendix

We present in this Appendix asymptotic analyses for small and large times of (4.8) for cooling a supereutectic melt from below. We assume that $\gamma = O(1)$ and $S = O(1)$. For small times, all variables will be small, and so we linearize to obtain

$$\psi \sim \tau, \qquad \theta \sim 1-\mathrm{e}^{-A\tau}. \tag{A 1a, b}$$

The initial thermal balance is between latent-heat production and heat conduction through the solid. This gives the leading-order behaviour for the thickness of solid

$$h \sim \left(\frac{2\gamma\tau}{S+1}\right)^{\frac{1}{2}}. \tag{A 2}$$

This solution holds until either h and $\psi = O(1)$, which occurs when $\tau \sim O(1, (S+1)/\gamma)$ or until $Ah(1-\theta)(1-\frac{1}{3}\psi) \sim O(\gamma)$, which occurs when $\tau \sim \gamma(1+S)/2A^2$.

We now consider the case in which $A \gg 1$, which corresponds to thermal-flux models I and III (§4.3). To proceed further in this case it is instructive to introduce the variables $\rho = A\tau$ and $d = he^{\rho}$ which yields

$$(S+\mathrm{e}^{-\rho})(dd_{\rho}-d^2)+d = \frac{\gamma}{A}\mathrm{e}^{2\rho} \quad \text{for} \quad h, \psi \ll 1. \tag{A 3}$$

In these variables the initial asymptotic regime is

$$\psi \sim 1-\mathrm{e}^{-\rho/A}, \tag{A 4}$$

$$\theta \sim 1-\mathrm{e}^{-\rho}, \tag{A 5}$$

$$d \sim \left(\frac{2\gamma\rho}{A(1+S)}\right)^{\frac{1}{2}}. \tag{A 6}$$

This solution breaks down when $\tau \sim O(\gamma(1+S)/2A^2)$ and then the dominant balance in the thermal equation is between the convective heat flux from the melt and the conductive heat flux across the solid, giving

$$d \sim \frac{\gamma}{A}\mathrm{e}^{2\rho}. \tag{A 7}$$

The nonlinear terms are not important in this regime because

$$dd_{\rho}-d^2 \sim \frac{\gamma^2}{A^2}\mathrm{e}^{4\rho} \ll \frac{\gamma}{A(1+S)}\mathrm{e}^{2\rho} \quad \text{if} \quad \mathrm{e}^{2\rho} \ll \frac{A}{\gamma}\left(\frac{1}{1+S}\right).$$

The approximations (A 4, A 5) for θ and ψ are still valid even though the form of the solution for h has changed. When $\rho \sim O(1)$ the linear balance in the energy equation breaks down. The melt has now cooled down sufficiently that the latent-heat production again balances the heat transfer across the solid. This third growth regime for h begins when $e^{2\rho} \sim A/[\gamma(1+S)]$ and $d \sim 1/(1+S)$. At this point $h \ll 1$ and $\tau \ll 1$ and therefore the asymptotic solutions for θ and ψ of regime 1 again apply. The linear term in the equation

$$(S+e^{-\rho})(dd_\rho - d^2) + d = \frac{\gamma}{A} e^{2\rho} \tag{A 8}$$

is not important and the nonlinear terms dominate, giving rise to the solution

$$d \sim \left(\frac{2\gamma}{AS}(\rho-\rho_0) + d^2(0)\, e^{-2\rho_0}\right)^{\frac{1}{2}} e^{\rho}. \tag{A 9}$$

Here $d(0)$ and ρ_0 may be evaluated by matching regimes 2 and 3. Hence

$$h \sim \left(\frac{2\gamma}{AS}(\rho-\rho_0) + d^2(0)\, e^{-2\rho_0}\right)^{\frac{1}{2}}. \tag{A 10}$$

This solution regime applies until $\tau \sim O(1)$ at which point the asymptotic approximation for ψ breaks down.

These three asymptotic forms for h may be seen on figure 6, which gives the numerical solutions for h, θ and ψ as functions of time and ϕ as a function of depth in the solid. Before the depth becomes $O(1)$, the approximation for ψ breaks down when $\tau \sim O(1)$ and the 4th regime begins. However, the solution for h given by regime 3 still holds. For $A \gg 1$, this change to regime 4 occurs after the change from regime 2 to 3, which happens when

$$\tau \sim \frac{1}{2A} \log\left(\frac{A}{\gamma(1+S)}\right).$$

For the 4th regime we introduce the variables δ and μ where

$$\delta = 1-\psi, \quad \mu = 1-\theta, \quad \delta, \mu \ll 1.$$

The non-dimensionalized equations (4.8) reduce to

$$h_\tau(S+\mu) + A\mu\delta^{\frac{1}{3}} = \frac{\gamma}{h}, \quad (1-h)\,\delta_\tau = -\delta^{\frac{4}{3}}, \tag{A 11 a, b}$$

$$(1-\delta-\phi)\,h_\tau = \delta^{\frac{4}{3}}, \quad (1-h)\,\mu_\tau = -A\mu\delta^{\frac{1}{3}} \tag{A 11 c, d}$$

giving $\mu = \mu_4(\delta/\delta_4)^A$, where δ_4 and μ_4 are obtained by matching regimes 3 and 4. Using the solution for h given in regime 3, it is found that

$$\delta \sim \left[\frac{1}{\delta_4^{\frac{1}{3}}} - \frac{S}{3\gamma}\left(\log\left(\frac{1-h}{1-h_4}\right) + (h-h_4)\right)\right]^{-3}. \tag{A 12}$$

The solution for h given in regime 3 is still asymptotic because the relevant thermal equation is now

$$h_\tau(S+\mu) + A\mu\delta^{\frac{1}{3}} = \frac{\gamma}{h}. \tag{A 13}$$

Here, the term $A\mu\delta^{\frac{1}{3}}$ representing the heat transfer from the melt is negligible.

The above analysis describes the evolution of the temperature and composition of the melt and thickness of the solid in the four different growth regimes. The

composition of the solid grown varies according to each of these asymptotic regimes.

In regime 1, the composition is of the form

$$\phi \sim \tau - \left(\frac{2(1+S)\tau}{\gamma}\right)^{\frac{1}{2}}. \tag{A 14}$$

In this quenching phase the composition increases as the solid grows. When the heat flux from the melt becomes more important than the rate of production of latent heat, this solution merges into regime 2. At the start of regime 2, the growth rate decreases to a minimum when little latent heat is required. This produces a maximum in the solid composition, as there is more time for crystals of component B to be deposited owing to the compositional flux. After merging to regime 2, $d \sim (\gamma/A)\,\mathrm{e}^{2\rho}$ and so $h \sim (\gamma/A)\,\mathrm{e}^{\rho}$ giving $h_\tau \sim \gamma\,\mathrm{e}^{\rho}$. Thus at the start of regime 2, $h_\tau \sim \gamma$ and $\phi \sim -1/\gamma$. For comparison, the numerical result shows that the maximum composition corresponds to $\phi \sim -9$ whereas the asymptotic analysis predicts that $\phi \sim -10$ for the parameters of figure 6(*c*) ($S = 10$, $\gamma = 0.1$); this partially confirms the validity of the solutions. Beyond this point in regime 2, the solid thickness increases exponentially and its composition decreases. The composition will be of the form

$$\phi \sim \tau - \frac{1}{\gamma}\left(1 - \frac{4\tau}{3}\right)\mathrm{e}^{-\tau A}. \tag{A 15}$$

At the end of regime 2, this has the value

$$\phi \sim -\frac{1}{\gamma}\left(\frac{\gamma(1+S)}{A}\right)^{\frac{1}{2}}, \tag{A 16}$$

where

$$\mathrm{e}^{\rho} \sim \left(\frac{A}{\gamma(S+1)}\right)^{\frac{1}{2}}. \tag{A 17}$$

Regime 3 then gives a third asymptotic form for ϕ, that

$$\phi \sim \tau - \left(\frac{S}{\gamma}\right)\left(1 - \frac{4\tau}{3}\right)\left(\frac{2\gamma}{AS}(\rho - \rho_0) + d^2(0)\,\mathrm{e}^{-2\rho_0}\right)^{\frac{1}{2}}. \tag{A 18}$$

Thus ϕ decreases again, corresponding to an increase in the composition of the solid being grown. This occurs because the solid growth rate decreases now that the latent-heat production balances the heat transfer across the solid. Therefore the compositional flux, which has not yet decayed significantly, has more time to supply composition to the solidifying material. However, regime 3 merges into regime 4 when the rate of decrease of the compositional flux exceeds the rate of decrease of the solid growth rate and the solid composition falls. This may be seen in the asymptotic form of the solution for regime 4

$$\phi \sim 1 - \left[\frac{1}{\delta^{\frac{1}{4}}} - \frac{S}{3\gamma}\left(\log\left(\frac{1-h}{1-h_4}\right) + (h - h_4)\right)\right]^{-3} - \frac{Sh}{\gamma}\left[\frac{1}{\delta^{\frac{1}{4}}} - \frac{S}{3\gamma}\left(\log\left(\frac{1-h}{1-h_4}\right) + h - h_4\right)\right]^{-4}. \tag{A 19}$$

The decrease of melt composition and consequently the solid composition occurs over a timescale of order $\tau \sim O(S/2\gamma)$ which is the time over which the melt solidifies as a whole. Thus the stratification produced by this process will extend over a significant thickness of the solid. When $A = O(\kappa_{\mathrm{m}}/D)$, which corresponds to thermal

model I, the following solid thicknesses are predicted for $S = 4.25$, $\gamma = 0.3$ and $\kappa_m/D = 100$:

Asymptotic regime	Timescale	Thickness grown
1	2.2 s	0.07 cm
2	9 min	0.53 cm
3	7.7 hr	7.7 cm
4	2 days	12 cm

Whereas when $A = O((\kappa_m/D)^{\frac{1}{2}})$, which corresponds to thermal model III, the following values are predicted:

Asymptotic regime	Timescale	Thickness grown
1	4 min	0.66 cm
2	43 min	1.0 cm
3	7.7 hrs	7.4 cm
4	2 days	12 cm

Now we consider the case $A = O(1)$. When $A = 1$ equations A 11 (b), (d) give

$$\theta = \psi, \tag{A 20}$$

which simplifies the equations to

$$h_\tau(1+S-\psi)+(1-\psi)^{\frac{4}{3}} = \frac{\gamma}{h}, \tag{A 21a}$$

$$(1-h)\,\psi_\tau = (1-\psi)^{\frac{4}{3}}, \quad (\psi-\phi)\,h_\tau = (1-\psi)^{\frac{4}{3}}. \tag{A 21b,c}$$

For small times, the same linearized asymptotic equations hold as given in the previous case (regime 1):

$$\psi \sim \tau, \quad h \sim \left(\frac{2\gamma\tau}{(S+1)}\right)^{\frac{1}{2}}, \quad \phi \sim \tau - \left(\frac{2\tau(S+1)}{\gamma}\right)^{\frac{1}{2}}, \tag{A 22a–c}$$

and the solution remains valid until $\tau \sim O(1)$, $\tau \sim O((1+S)/2\gamma)$ or $\tau \sim O(\frac{1}{2}(S+1)\,\gamma)$. It fails initially when $\tau \sim O(1)$ (we assume that $\frac{1}{2}(S+1)\gamma = O(1)$) and the solution enters the second asymptotic regime. The dominant balance in the thermal equation is now

$$hh_\tau = \frac{\gamma}{S}. \tag{A 23}$$

However, the composition and temperature fields in the melt now evolve as

$$\psi \sim 1-\left(1-\frac{S}{3\gamma}\left[\log\left(1-\left(\frac{2\gamma\tau}{S}\right)^{\frac{1}{2}}\right)+\left(\frac{2\gamma\tau}{S}\right)^{\frac{1}{2}}\right]\right)^{-3}. \tag{A 24}$$

This solution holds until the composition and temperature in the melt have decayed to eutectic, at which time the solid depth will be of order 1. As before, the composition evolves as

$$\phi \sim \tau - \left(\frac{2S\tau}{\gamma}\right)^{\frac{1}{2}} \tag{A 25}$$

in the initial quench solution. However, in the second asymptotic regime, the composition evolves as

$$\phi \sim 1-\left(1-\frac{S}{3\gamma}\left[\log\left(1-\left(\frac{2\gamma\tau}{S}\right)^{\frac{1}{2}}\right)+\left(\frac{2\gamma\tau}{S}\right)^{\frac{1}{2}}\right]\right)^{-3} - \left(\frac{2S\tau}{\gamma}\right)^{\frac{1}{2}}\left(1-\frac{S}{3\gamma}\left[\log\left(1-\left(\frac{2\gamma\tau}{S}\right)^{\frac{1}{2}}\right)+\left(\frac{2\gamma\tau}{S}\right)^{\frac{1}{2}}\right]\right)^{-4}, \tag{A 26}$$

which is equivalent to regime 4 of the previous problem. Thus the composition falls to eutectic over a time of order $\tau \sim S/2\gamma \sim 4$. The numerical solution for $A = 2$ shown in figure 7 indicates that $\psi \sim 1$ and $h \sim 0.8$ when $\tau \sim 5$, which agrees with the order-of-magnitude analysis. Above $h \sim 0.8$, $\phi \sim 1$ ($S = 4.25$, $\gamma = 0.56$).

REFERENCES

ADORNATO, P. M. & BROWN, R. A. 1987 Convection and segregation in directional solidification of dilute and non-dilute binary alloys: effects of ampoule and furnace design. *J. Cryst. Growth* **80**, 115.

CARSLAW, H. S. & JAEGAR, J. C. 1986 *Conduction of Heat in Solids*. Oxford University Press.

CHEN, C. F. & TURNER, J. S. 1980 Crystallisation in a double-diffusive system. *J. Geophys. Res.* **85**, 2573.

CORIELL, S. R., CORDES, M. R., BOETTINGER, W. J. & SEKERKA, R. F. 1981 Convective and interfacial stability during unidirectional solidification of a binary allow. *J. Cryst. Growth* **49**, 13.

ELLIOTT, R. 1983 *Eutectic Solidification Processing*. Butterworths.

FOWLER, A. C. 1985 The formation of freckles in binary alloys. *IMA J. Appl. Maths.* **35**, 159.

HOWARD, L. N. 1964 Convection at high Rayleigh number. *Proc. 11th Intl Cong. Appl. Mech.*, p. 1109. Springer.

HUPPERT, H. E., SPARKS, R. S. J., WILSON, J. R., HALLWORTH, M. A. & LEITCH, A. M. 1987 Laboratory experiments with aqueous solutions modelling processes in a magma chamber II. Cooling and crystallization along inclined planes. In *Origins of Igneous Layering* (ed. I. Parsons), p. 539. Reidel.

HUPPERT, H. E. & WORSTER, M. G. 1985 Dynamic solidification of a binary alloy. *Nature* **314**, 703.

HURLE, D. T. J. & JAKEMAN, E. 1968 Morphological stability of lamellar eutectics. *J. Cryst. Growth* **3–4**, 594.

HURLE, D. T. J., JAKEMAN, E. & WHEELER, A. A. 1982 Effect of solutal convection on the morphological stability of a binary alloy. *J. Cryst. Growth* **58**, 163.

KERR, R. C. 1984 Crystallisation and compositional convection in geological fluid mechanics. Ph.D. thesis, Cambridge University.

KRISHNAMURTI, R. 1970 On the transition to turbulent convection. *J. Fluid Mech.* **42**, 295.

KURZ, W. & FISHER, D. J. 1986 *Fundamentals of Solidification*. Trans Tech Publishers.

LANGER, J. S. 1980 Instabilities and pattern formation in crystal growth. *Rev. Mod. Phys.* **52**, 1.

LEITCH, A. M. 1985 Laboratory models of magma chambers. Ph.D. thesis, A.N.U., Canberra, Australia.

LINDEN, P. F. & SHIRTCLIFFE, T. G. L. 1978 The diffusive interface in double-diffusive convection. *J. Fluid Mech.* **87**, 417.

MCBIRNEY, A. R. & NOYES, R. M. 1979 Crystallisation and layering of the Skaergaard intrusion. *J. Petrol.* **20**, 487.

MOLLARD, F. R. & FLEMINGS, M. C. 1967 Growth of composites from the melt, Parts I and II, Trans. Met., AIME **239**, 1526 and 1534.

MULLINS, W. W. & SEKERKA, R. F. 1964 Stability of a planar interface during the solidification of a binary alloy. *J. Appl. Phys.* **35**, 444.

TURNER, J. S. 1979 *Buoyancy Effects in Fluids*. Cambridge University Press.

TURNER, J. S., HUPPERT, H. E. & SPARKS, R. S. J. 1986 Komatiites II – experimental and theoretical investigations of post emplacement cooling and crystallisation. *J. Petrol.* **27**, 397.

WEAST, Q. C. (ed.) 1971 *Handbook of Chemistry and Physics*. Cleveland: C.R.C.

WORSTER, M. G. 1983 Convective flow problems in geological fluid mechanics. Ph.D. thesis, Cambridge University.

WORSTER, M. G. 1986 Solidification of an alloy from a cooled boundary. *J. Fluid Mech.* **167**, 481.